CHARACTERIZATION AND MODELING OF A HIGH-PRESSURE WATER-FOGGING SYSTEM FOR GRAIN DUST CONTROL

D. Brabec, R. Maghirang, M. Casada, E. Haque

ABSTRACT. *Grain dust, a health and safety risk, is generated whenever grain is loaded into or unloaded from hoppers and equipment. This research investigated airflow models and evaluated the particle dynamics from a high−pressure water−fogging system for potential dust control at a grain−receiving hopper. Experiments were performed in a test chamber, representing a narrow section of a grain−receiving hopper. A 0.2 mm (0.008 in.) spray nozzle was used to produce a plume of fog directed across a free−falling grain column. More than 90% of the fog droplets ranged from 10 to 40 μm in diameter. Average droplet velocities in the plume cross−section were over 10 m s^{-1} at 7.6 cm from the nozzle. The air−velocity pressures at 7.6 cm were parabolic in the radial direction, with maximum pressures over 275 Pa (1.1 in. H_2O). Airflow distributions, grain dust transport, and spray droplet trajectories within the test chamber were modeled in three dimensions using FLUENT, which is a computational fluid dynamics (CFD) software program. Induced airflow from the spray fog caused recirculation of the air and dust particles in the lower part of the chamber. This recirculation pattern transported the dust from the grain pile back into the spray plume, where it mixed with the spray fog. The spray produced deposits on the surface of the grain pile ranging from 0.1 to 0.4 mg cm^{-2} s^{-1}. However, when the grain pile filled the chamber and was positioned directly in the spray plume, the grain surface deposits were 1.2 mg cm^{-2} s^{-1} at the grain peak. The spray produced deposits on the sidewall of the chamber. Sidewall spray deposits were 11 mg cm^{-2} min^{-1} in the middle of the test chamber and 1.5 mg cm^{-2} min^{-1} near the outlet. The sidewall dust deposits during spray treatment ranged from 1.2 to 0.5 mg cm^{-2} min^{-1} and correlated with the spray deposits with an R^2 of 0.95.*

Keywords. *CFD, drops, mist, particles, spray.*

The amount of airborne dust generated during grain handling varies with grain type, grain condition, and handling methods. Workers exposed to dusty environments can develop respiratory problems. Grain elevator employees have experienced reduced lung function depending on individual sensitivity and dust exposure (Enarson et al., 1985). High concentrations of dust in grain facilities and equipment provide fuel for potential flash fires or dust explosions. Annually, an average of 12 grain dust−related fires/explosions of varying intensity was reported from 1992 to 2001 in the U.S. (Schoeff, 2002).

Primary methods for controlling dust emissions in grain handling facilities are pneumatic dust−collection systems and direct application of food−grade oils to grain streams. Each method has its advantages and limitations, as cited by the U.S. Congress' Office of Technology Assessment (1995). The dust−capture efficiency of a pneumatic system varies with airflow and proximity of the dust to the collecting hood. Pneumatic systems are expensive to install, maintain, and operate. Oil additives, while not effective at the initial point of application, are effective after initial mixing and at later transfer points. However, oiled grain has been reported as adversely affecting milling processes (Reid, 1987).

High−pressure water−spray systems, which produce jets of fog and mist, have demonstrated some potential to confine and suppress grain dust (Brabec, 2003). The spray−fog differs from coarse−spraying systems because the water amount is reduced and the droplet size is decreased. Use of spray systems should take into account the fact that U.S. law forbids the addition of water to merchandised grain shipments for the purpose of adding weight (Federal Register, 1994), although water addition is allowed for some processes (e.g., tempering wheat) and pesticide application. Further investigation was needed to characterize spray−fog systems, including droplet−size distribution and rates of induced airflows, and to determine the effects of the water fog on the grain and equipment. Investigations may be done through experimental research using full−scale or small−scale prototypes and using computational fluid dynamics (CFD).

Previous researchers have demonstrated the applicability of CFD in predicting airflow within structures such as greenhouses (Al−Arifi et al., 2001) and swine buildings (Sun et al., 2002). Additionally, Brown and Sidahmed (2001) have analyzed spray systems using CFD. They found that the measured and CFD simulated deposits from the forestry

Article was submitted for review in January 2004; approved for publication by the Structures & Environment Division of ASAE in November 2004.

Contributions from the Kansas State University Agricultural Experiment Station No. 04−089−J.

The authors are **Daniel Brabec, ASAE Member Engineer,** Engineering Technician, USDA−ARS Grain Marketing and Production Research Center, Manhattan, Kansas; **Ronaldo Maghirang, ASAE Member Engineer,** Professor, Department of Biological and Agricultural Engineering, Kansas State University, Manhattan, Kansas; **Mark Casada, ASAE Member Engineer,** Research Engineer, USDA−ARS Grain Marketing and Production Research Center, Manhattan, Kansas; and **Ekramul Haque, ASAE Member Engineer,** Professor, Department of Grain Science, Kansas State University, Manhattan, Kansas. **Corresponding author:** Daniel Brabec, USDA−ARS Grain Marketing and Production Research Center, 1515 College Ave., Manhattan, KS 66502; phone: 785−776−2731; fax: 785−776−2792; e−mail: dan@gmprc.ksu.edu.

air−blast sprayer were generally in good agreement. However, some discrepancies were observed with 24 to 70 μm droplets. Tsay et al. (2002) used CFD simulation to study drift potential from an agricultural field sprayer containing shields and its effectiveness at various ground speeds and ambient wind directions. Kwok (1991) presented some basic information on air and droplet movement from a spray.

OBJECTIVES

The objectives of this study were to: (1) characterize the droplet size and airflow distributions of a high−pressure water−fog system, and (2) model airflow distribution, particle trajectories, and droplet trajectories from spray fogs in a pilot−scale grain−receiving hopper using three−dimensional CFD.

MATERIALS AND METHODS

Experiments were performed to characterize the airflow and droplet−size distribution of a spray fog. Qualitative airflow observations were made with smoke test, while quantitative airflow measurements were performed with a pitot tube. Two nozzles were sent to a private laboratory for droplet size and velocity measurements. Experiments (Brabec et al., 2004) were performed with a test chamber containing incoming grain and the spray fog to study the effectiveness of the system in reducing grain dust emission. CFD models were developed to describe airflow from an individual nozzle and from a line of seven nozzles within the test chamber receiving grain and during spray operations. Particle trajectories were calculated within the predicted chamber airflow profiles. Measurements were taken of the spray deposits on the grain surface and on the chamber sidewalls. The sidewall spray accumulations were modeled.

CHARACTERIZATION OF THE SPRAY SYSTEM

A complete spray system (model E1, Environmental Engineering Concepts, Palm Springs, Cal.) was used in this study. The system included the electric motor, controls, pump, pressure gauges, water filters, and lines with nozzles. The nozzles had orifices of 0.20 mm (0.008 in.) diameter, contained internal impellers, and produced fine sprays. The pump could operate from 5.5 MPa (800 psi) to over 8.3 MPa (1200 psi) with 10 to 60 nozzles.

Airflow Profile Associated with Individual Nozzles

Induced airflow was qualitatively investigated using smoke and photography. It was also quantified for an individual nozzle at 6.9 MPa using a pitot tube (model 160S, Dwyer Instruments, Michigan City, Ind.) and an inclined manometer (fig. 1). The nozzles were oriented horizontally into open space. Pressure data were collected at three horizontal sampling stations, located 7.6, 30.5, and 61 cm away from the nozzle orifice. At each station, measurements were made at vertical distances ranging from 0 to ±5.1 cm from the nozzle axis (horizontal centerline).

Droplet Size and Velocity Distributions for Individual Nozzles

Two randomly selected nozzles, from a group of 32 nozzles, were tested at a commercial laboratory (Spraying Systems Co., Wheaton, Ill.) to determine droplet size and velocity distributions. The nozzles were tested at the normal operating pressure of 6.9 MPa (1000 psi). The nozzles were directed horizontally into open space. A phase−doppler particle analyzer was used. In this instrument, a low−power laser beam splits, producing two laser beams that are redirected to intersect at the droplet sampling location. When a droplet passes through the intersection of the laser beams, a light−interference pattern is formed and detected by several parallel detectors. Droplet velocity and size are determined from the frequency information of the interference pattern and the phase−shift information from the detectors (Spraying Systems, 2000).

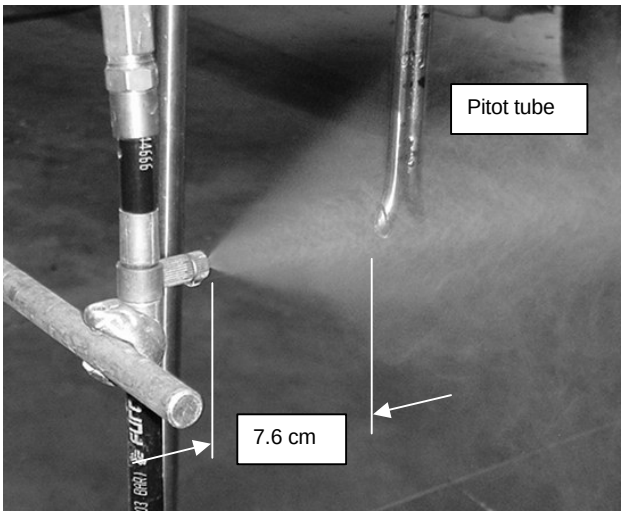

Figure 1. Air−pressure measurement from a single nozzle of a spray fog.

Spray samples were taken at 7.6 cm (3 in.) and 30.5 cm (12 in.) horizontally from the tip of the nozzle and consisted of 11 vertical test points across the plume at each station (fig. 2). The two horizontal positions were selected to demonstrate the changes in droplet size and velocity with distance from the nozzle. At 7.6 cm, the vertical test points extended symmetrically ±4.4 cm from the centerline of the nozzle. At 30.5 cm, the test points extended from 1.9 cm above the horizontal centerline of the nozzle to 12.7 cm below to include droplets falling out of the spray plume. During each 30 s sampling period, 30,000 drop data values were collected at each test location.

AIRFLOW MEASUREMENTS IN A TEST CHAMBER

A test chamber was setup to simulate a narrow portion of a grain−receiving hopper (fig. 3). The test chamber was

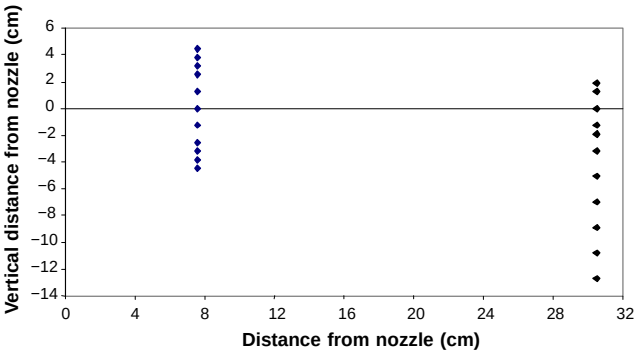

Figure 2. Locations where spray−fog droplet−size distributions were measured.

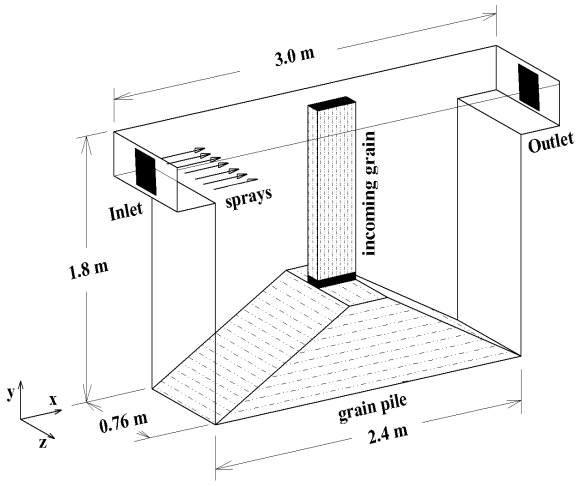

Figure 3. Three−dimensional outline of the test chamber showing the grain pile, incoming grain stream, inlet, outlet, and spray nozzles.

0.76 m wide × 3.0 m long × 1.8 m high with identical inlet and outlet openings. A line of seven nozzles was mounted at the inlet. The nozzles were spaced 10 cm apart and operated at 6.9 MPa. Corn was stored in an overhead bin and dropped into the test chamber at a rate of 2.55 m^3 min^{-1} (72 bu min^{-1}). The chamber's opening for grain was 20 × 30 cm, but the grain column required only half the opening. After each grain−drop/spray trial, the grain was emptied from the test chamber and cycled to an overhead bin.

Airflow was measured at the inlet and outlet using a 22 cm diameter propeller anemometer. The recirculating airflow pattern within the test chamber was recorded using a video camera and smoke. Smoke was injected into the test chamber at 30.5 cm below the chamber outlet while the spray system was operating. Video data were transferred from a video cassette player to a computer with an imaging circuit board and software (EPIX, Inc., Buffalo Grove, Ill.).

Spray−Fog Grain Surface Deposits

Experiments were performed to measure the fog deposits on the grain surface. The deposits were collected for three static levels of grain, while seven spray nozzles were operated. Grain levels were defined as the vertical distance from the nozzles down to the grain surface and were −138 cm (floor), −106 cm, and −60 cm. Grain was loaded into the test chamber at the specified level, and then droplet collection filters were placed at six locations on the grain pile. Three filter samples were evenly spaced on the front incline and three on the back incline of the grain pile. A wooden barrier, 10 cm deep × 30 cm wide × 180 cm high, was positioned in the middle of the test chamber to simulate the volume occupied by the incoming grain. The filters (CMS No. 263−806) had a diameter of 18.5 cm and an area of 268 cm^2. They were weighed on an electronic balance (model PC 180, Mettler, Hightstown, N.J.) before and after sampling. The spray was operated at 6.9 MPa and for 30 s per trial.

Spray Sidewall Deposits

Total deposits (grain dust and water droplets) on the wall of the test chamber were collected using sidewall filters while grain was dropped and the spray system was operated. Filters were weighed before (pre−trial), immediately after each trial

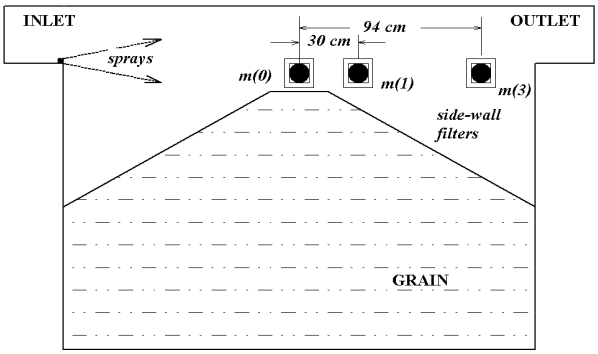

Figure 4. Schematic of the test chamber showing the sidewall sampling filter locations.

(wet filter), and after a drying period of 24 h (dried filter) using an electronic balance with a sensitivity of 0.1 mg (model 40SM−200A, Precisa Balance, Zurich, Switzerland). Dust deposits were determined by subtracting the pre−trial filter weight from the dried filter weight. Spray deposits were determined by subtracting the dried filter weight from the wet filter weight.

Three new deposition filters were used per trial. Sampling locations were 30 cm from the top of the chamber. The sampling locations started at the middle of the chamber where the largest deposits were observed and extended to the outlet (fig. 4). The following notations are defined for the sampling locations: m(0) = middle, m(1) = mid+30 cm, and m(3) = mid+94 cm. The filters (model PA41, Pall−Gelman, Ann Arbor, Mich.) had a diameter of 12.5 cm and were placed in filter holders having an 11.4 cm diameter opening, thus exposing an area of 102 cm^2.

CFD Modeling

Numerical simulations of airflow and particle movement and fate were accomplished using FLUENT (version 6.0, Fluent, Inc., Lebanon, N.H.). The geometry, grid, and boundary conditions were specified with FLUENT's geometry meshing software, GAMBIT. The geometry was three−dimensional and matched the dimensions of the test chamber. The grid system produced over 30,000 control volumes. Finer meshes were employed around the nozzles, inlet, and outlet.

CFD airflow models were computed for simulated conventional grain receiving, grain receiving with spray operations, and recirculating air and smoke tests. Pressure and velocity components were numerically determined from the discretized mass−continuity equation and the discretized *x*, *y*, and *z* conservation of momentum equations (Fluent, 2002). Air turbulence was simulated using a standard k−ε turbulence model, where k is the turbulent kinetic energy and ε is the turbulence dissipation rate. The standard k −ε turbulence model was developed over recent decades from a mixture of theoretical and empirical models to provide reasonable approximate deviations from the mean velocities. The standard k −ε turbulence model was used because the airflow was low, less than 5.6 m^3 min^{-1} (200 cfm). Swirling airflows, such as in large cyclones, use over 10 times that airflow and require a modified version of the turbulence model for more accurate results.

Calculation of the position and velocity components of dust particles and droplets accompanied most of the airflow

models. Trajectories were determined from the incremental changes of particle forces, accelerations, and velocities based on Newton's second law of motion. Using FLUENT's Discrete Random Walk (DRW) model, the effects of Stoke's drag force (Hinds, 1982) and the force of gravity were computed after each 1.8 mm change in position. The DRW adjusted the local average velocities with the computed turbulent velocity variations. The effect of evaporation was not considered in these models because observations showed that evaporation was a minor factor for the spray test setup and test environment (eastern Kansas).

Some of the basic model assumptions were three−dimensional motion, steady−state flow, and isothermal conditions. The ambient air conditions were 27˚C and atmospheric pressure. The following two assumptions were also made:

- The spray consisted of two parts: an air source, which was located 7.6 cm from the nozzle, and a group of droplets.
- The entrained air (with the incoming grain), which was modeled as a small air source near the top of the grain pile, was directed horizontally at the top of the grain pile because it could not advance further.

Modeling Airflow from Grain Receiving

Details of the model and boundary conditions (B1 to B7) are shown in figures 5 and 6 and table 1. The test chamber geometry contained a subsection representing the incoming grain column. The grain column (B5) was modeled as a wall moving at 1.4 m s^{-1} downward with a wall friction constant of 0.5. This velocity was determined by dividing the grain flow rate into the chamber (2.55 m^3 min^{-1}) by the cross−sectional area of the grain column (10 × 30 cm).

The grain pile boundary (B3) was a fixed boundary with a specified air velocity source having a constant velocity of 2.5 cm s^{-1} (fig. 5, Air1). This displaced air source was actually caused by the rise of the grain pile with the incoming grain, which was approximately 2.5 cm s^{-1}. The airflow from the test chamber was observed to be greater than the grain's volumetric flow rate. This difference between the measured airflow and volumetric grain flow was considered entrained air. Air was entrained with the incoming grain at a rate of 0.34 m^3 min^{-1} for corn entering at 2.55 m^3 min^{-1} (Brabec, 2003).

The bottom 6 cm of the grain column was considered the impact zone with the top of the grain pile. At this location, the entrained air (B4) was redirected normal to the grain column rather than injected into the grain pile. The entrained airflow provided a source to transport the grain dust. The air velocity from the impact zone (fig. 5, Air2) was estimated as 0.12 m s^{-1} and was determined by dividing the volume of the entrained air by the cross−sectional area of the estimated impact zone. This area is normal to the Air2 velocity (fig. 5) and is equal to the circumference of the grain column cross−section times the height of the impact zone. The height of the impact zone was estimated from observations.

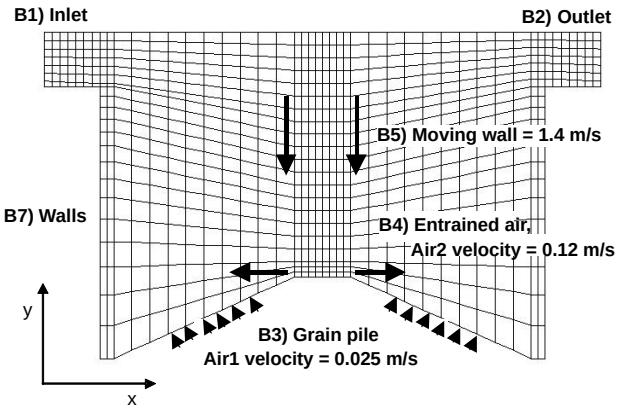

Figure 5. A two−dimensional schematic view showing the computational domain of the test chamber, grid pattern, and boundary conditions (B1 to B7, explained in table 1).

Modeling Dust During Grain Receiving with Spray Operations

An array of grain dust particle sizes were tracked (diameter d_p = 5 to 40 μm, density of 1.5 g cm^{-3}). Particle sizes were based on the measured size distribution of corn dust samples taken with a high−volume air sampler during grain−drop tests. As an initial condition, the particles were released at an angle of 45˚ above the horizontal and at 1.4 m s^{-1} from 56 evenly spaced locations around the four sides of the impact zone. The total mass flow of the dust was 24 g min^{-1}. The discrete−phase model then calculated the position of the particles after each 1.8 mm of movement.

Modeling Airflow from a Spray Nozzle

Each nozzle was defined as a cross−sectional area (fig. 6) and a pressure source that produced airflow similar to that of a single nozzle. Pressure source was based on air−velocity pressure measurements taken 7.6 cm from individual nozzles operating at 6.9 MPa. For the CFD model, seven nozzles were specified. Each nozzle's cross−sectional area was 18 × 18 mm, and its velocity pressure was 200 Pa.

Modeling Droplet Fates

The spray was simulated in CFD as a truncated cone at each nozzle location. The cone radius was 4 cm and the cone angle was 40˚. Droplets of 18 μm diameter and 1 g cm^{-3} density were released with 10 m s^{-1} velocity at the given cone angle and directed into the test chamber. Each cone was com−

Table 1. Boundary conditions applied to the test chamber.

	Boundary Descriptions		Size	Turbulence	
Geometry	Variable	Value	(m × m)	Intensity (%)	Length (m)
B1) Inlet	Pressure inlet	1 atm	0.25 × 0.25	2	0.24
B2) Outlet	Pressure outlet	1 atm	0.25 × 0.25	3	0.24
B3) Grain pile	Velocity inlet	0.025 m s^{-1}	0.76 × 2.65	0.5	0.76
B4) Grain impact zone	Velocity inlet	0.12 m s^{-1}	0.06 × 0.8 (circ.)[a]	5	0.03
B5) Grain column	Moving wall	1.4 m s^{-1}	1.34 × 0.8 (circ.)[a]		
B6) Individual nozzles	Fan	200 Pa	0.018 × 0.018		
B7) Walls	Wall	default			

[a] 0.8 (circ.) represents the circumference of the grain column.

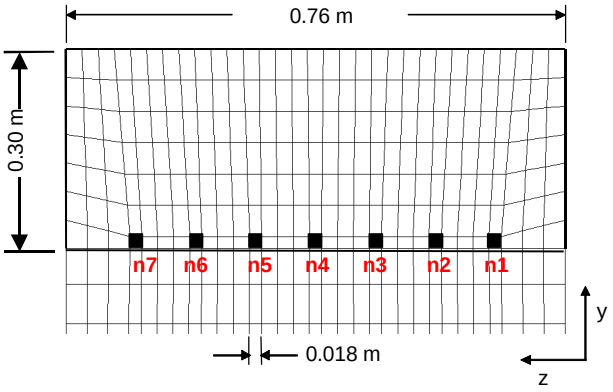

Figure 6. Cross−section of the top portion of the chamber inlet. showing the arrangement of the seven spray nozzles (black squares).

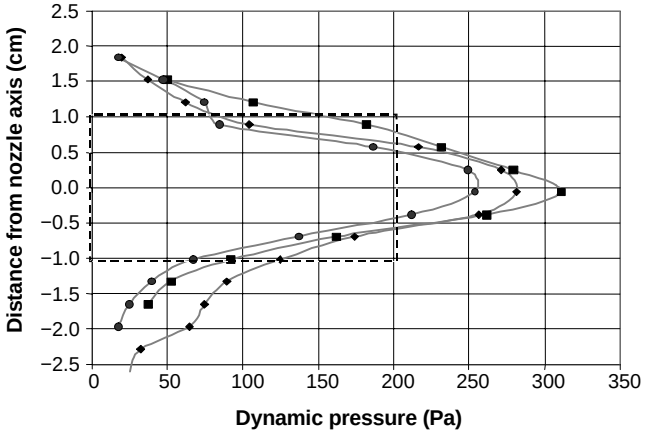

Figure 7. Air−velocity pressure profiles for three nozzles at 6.9 MPa.

posed of 32 injection positions. The liquid mass flow from each nozzle was 90 g min^{-1} and was distributed among the 32 injection points of each nozzle. The discrete−phase model was limited to a maximum of 3500 steps completed in a maximum of 12 s of particle motion. Trajectories were computed for 9600 droplets from each nozzle location. Predicted results were expressed in terms of the percentage of droplets that had escaped through the outlet, were trapped on a surface, or remained drifting within the test chamber after 12 s of computations.

From these results, the fraction of droplets that deposited on sidewall virtual filters was determined. These filters were 30 × 30 cm and were located at the same horizontal positions (0, 30, and 94 cm from the middle of the incoming grain) as the actual filters (fig. 4). These virtual filters were also referred to as m(0), m(1), and m(3), respectively. A relative deposit was computed for m(0) and m(1) by dividing each surface deposit estimate by the surface deposit m(3).

Results and Discussion

Induced Airflow from the Spray

Induced airflow was analyzed qualitatively using a smoke plume generated from a smoke stick. When the smoke plume entered the underside of the spray, the entire plume was swept to one side and diffused with the spray. In contrast, when smoke was directed under a metal screen in stationary air, most of the smoke passed through the porous screen. With the spray fog, the induced air redirected particle movement.

In figure 7, the pitot tube measurements of individual nozzles show that the maximum air−velocity pressure for three nozzles at 7.6 cm was greater than 250 Pa (1.0 in. H_2O). The average measured pressure is shown by the dashed rectangle. The pressure profile is parabolic with a base width of approximately 3 to 4 cm. Maximum air−velocity pressures at 15.2, 30.5, and 61.0 cm from the nozzle tip were approximately 110, 42, and 12 Pa, respectively.

Spray Droplet Size and Velocity Distributions

Measured droplet size and velocity varied with horizontal and vertical locations in the spray plume. Volumetric median diameters ($D_{V0.5}$) for two nozzles at 7.6 cm (3 in.) and 30.5 cm (12 in.) from the nozzle tip, and for all vertical test locations across the spray plume, are shown in figure 8. Both nozzles have similar size distributions. At 7.6 cm, the droplets have a $D_{V0.5}$ ranging from 15 to 25 μm. Observed liquid flow distribution across the spray plume at 7.6 cm from the tip depicted a hollow−cone spray with most of the droplets located at ±3.8 cm (1.5 in.) from the centerline. At 30.5 cm from the nozzle and within the plume, the droplet $D_{V0.5}$ ranged from 20 to 35 μm. However, at 30.5 cm from the nozzle and at 8 cm below the nozzle centerline, the droplet $D_{V0.5}$ dramatically increased to over 150 μm because droplets had agglomerated and fallen out.

The variations in droplet sizes at the single sampling point are given as droplet−size distributions (fig. 9 and table 2). This sampling point was located 7.6 cm from the nozzle tip and 3.8 cm below centerline. Approximately 98% of the spray volume ranged from 10 μm to 40 μm. Volumetric distribution was bimodal with peaks at 19 μm and 31 μm diameter. Count distribution indicates that 70% of the droplets were approximately 18 μm (13, 16, 19, and 22 μm bins). Each droplet diameter bin has an interval of 3 μm.

Average droplet velocities for the spray plume for the 22 sampling locations are shown in figure 10. The highest average droplet velocity was 11.5 m s^{-1} at 7.6 cm from the nozzle and 5.8 m s^{-1} at 30.5 cm. Average droplet velocity decreased in the direction of flow as droplet momentum was exchanged with the air.

Table 2 is one of 44 individual data sheets from the phase−doppler particle analyzer measurements. Each sheet

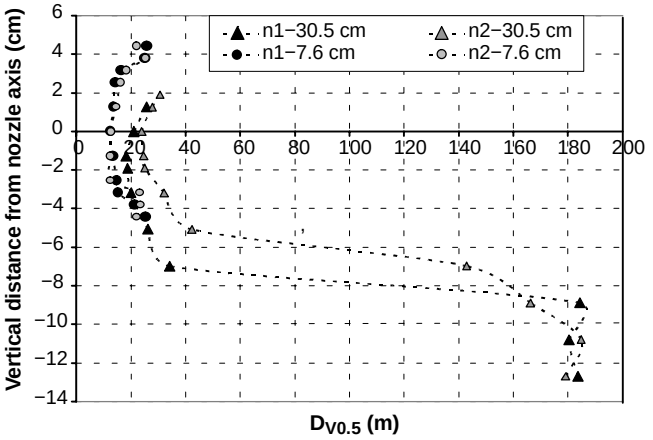

Figure 8. Volumetric median diameter ($D_{V0.5}$) from two nozzles (n1 and n2 in fig. 3) operated at 6.9 MPa. Measurements were made at 7.6 and 30.5 cm from nozzle orifice.

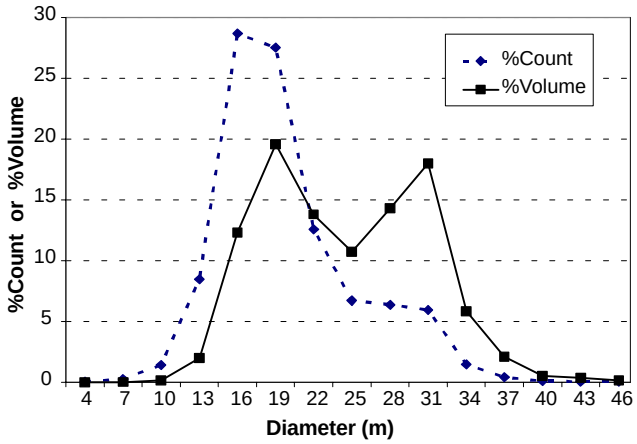

Figure 9. Droplet−size distribution at 7.6 cm from nozzle tip and at 3.8 cm below the centerline.

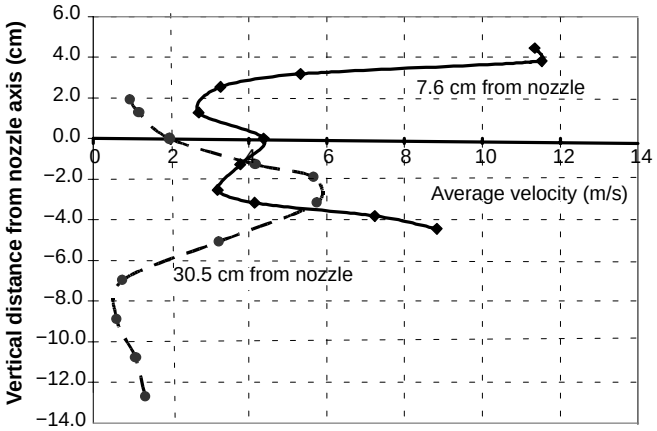

Figure 10. Mean droplet velocities for a nozzle at 6.9 MPa.

accounts for the measurements of 30,000 droplets. This data was collected at a location 7.6 cm from the nozzle and 3.8 cm below its centerline. At this location, the overall average droplet velocity was 7.2 m s^{-1}. However, droplets larger than 28 μm had velocities ranging from 18.8 to 25.7 m s^{-1}. These larger drops were still providing momentum to the air. The spray had an air velocity of approximately 18 m s^{-1} at this particular location while regarding its parabolic profile.

Table 2. Droplet diameter, velocities, counts, and volumes for a single test at a location 7.6 cm from the nozzle and 3.8 cm below the nozzle axis.

	Velocity		Cumulative	
Diameter (μm)	Average (m s^{-1})	Std. Dev. (m s^{-1})	Count (%)	Volume (%)
4.3	2.5	1.2	0.0	0.0
7.3	2.5	1.4	0.3	0.0
10.2	2.7	2.2	1.7	0.2
13.2	2.8	1.7	10.2	2.1
16.2	3.3	2.1	38.9	14.4
19.2	4.5	2.9	66.4	34.0
22.1	7.4	4.2	79.0	47.8
25.1	12.6	5.0	85.7	58.6
28.1	18.8	5.2	92.1	72.9
31.1	22.0	4.4	98.0	90.8
34.0	24.0	5.6	99.5	96.6
37.0	23.8	7.4	99.9	98.7
40.0	25.7	6.2	100.0	99.2
42.9	18.0	12.3	100.0	99.6

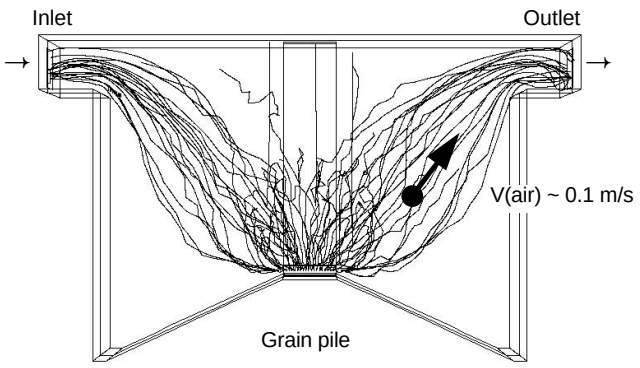

Figure 11. Predicted trajectories of grain dust particles from the grain impact zone when there was no spray (d_p = 14 μm, ρ_p = 1.5 g cm^{-3}, n = 72).

CFD Airflow and Particle Emission Modeling at Grain Receiving

Airflow and dust movement were predicted for the control case, i.e., grain dropping in the test chamber without spray application. Laboratory measurements of particle distributions of emitted dust samples indicated a geometric mean and standard deviation of 12.2 and 1.4 μm, respectively, and a maximum emitted particle size of approximately 25 μm, based on the particle size distribution from the dust sample collected at the outlet. Predicted results showed that the air and 14 μm dust particles exhausted from both the inlet and outlet of the test chamber (fig. 11).

CFD particle−tracking models estimated the maximum size near 40 μm based on % trapped (table 3). The size and airflow of the grain impact zone was estimated from observations and could be modified to further improve the predicted maximum particle size. If the grain impact zone area were increased for a given entrained airflow, then the escape velocities would have been lower and the maximum particle size would have reduced.

CFD Airflow and Particle Trajectories During Spray Operations

When the line of seven nozzles was added to the control test case, the airflow pattern was changed to a crossflow at the top of the chamber. Additionally, a fraction of the air was exhausted through the outlet and a fraction recirculated down the back wall and toward the inlet side. Predicted trajectories of the 18 μm droplets illustrate this recirculating airflow pattern (fig. 12a). Several factors potentially affect the

Table 3. Predicted fate of dust particles released from the grain pile impact zone when there was no spray. Results were from 5600 trajectory calculations per particle size.

Size	Average (%)		
(μm)	Escaped	Trapped	Drifted
5	73	10	16
8	74	12	14
12	74	12	14
15	73	13	14
20	63	19	18
25	39	49	12
30	16	83	1
40	2	98	0

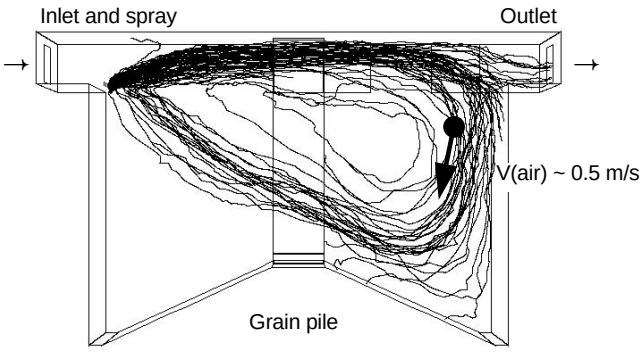

Figure 12a. Predicted trajectories of spray droplets during spray operation. Droplets (d_p = 18 μ m, ρ_p = 1 g cm^{-3}, n = 64) were released from the middle nozzle (n4 in fig. 3) during the presence of incoming grain and induced airflow from all nozzles.

recirculation, such as direction of the spray, pressure of the spray, and confinement of the spray.

Due to the recirculating airflow pattern associated with the spray, dust particles from the grain pile moved toward the spray nozzles and entered the spray plume near the tips of the nozzles (fig. 12b). Airflow near the grain pile changed considerably with the spray. The new airflow profile could have affected the amount and size of grain dust emitted. Possibly, less dust was emitted from the pile since the spray fog recirculated and closely covered the top of the grain pile. In addition, the potential for dust and droplet interaction was enhanced, since the dust particles were concentrated and mixed with the spray near the nozzles, where the spray was concentrated.

Table 4 summarizes the predicted fate of 18, 30, and 180 μm droplets for all nozzles. Approximately 49% to 53% of the 18 μm and 30 μm droplets were trapped on some surface, while 29% to 31% were still drifting after 12 s of computation. The 18 μm and 30 μm droplets were released

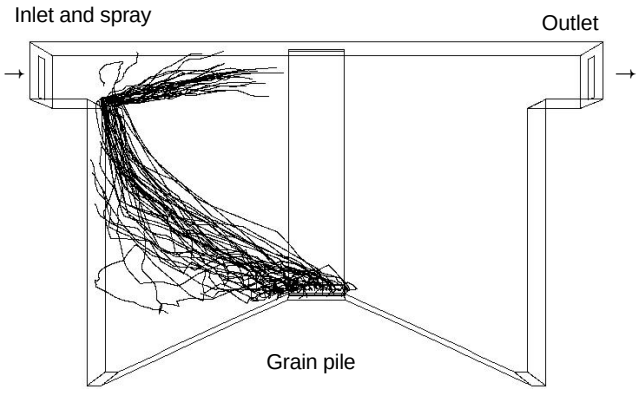

Figure 12b. Predicted trajectories of grain dust particles during spray operation. Particles (d_p = 14 μ m, ρ_p = 1.5 g cm^{-3}, n = 72) were released at the grain pile.

Table 4. Predicted fates of spray droplets from all nozzles (n1 to n7 in fig. 3).

	Droplet Size (μm)		
Fate	18	30	180
Escaped (%)	22	16	0
Drifted (%)	29	31	0
Trapped (%)	49	53	100

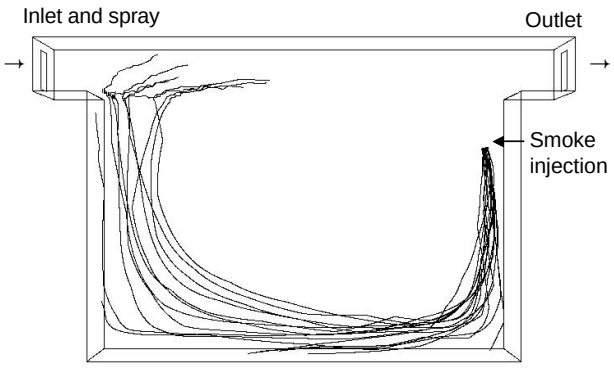

Figure 13. Smoke tracking in a simplified CFD model. Particles of 1 μm diameter and 1 g cm^{-3} density were released 30 cm below the outlet.

from seven nozzle locations with 9600 tracking events per nozzle location.

The predicted airflow pattern associated with the spray fog was validated qualitatively using smoke. To simplify the model geometry, the grain pile was removed and a short stream of smoke particles (d_p = 1 μ m, ρ_p = 1 g cm^{-3}) was injected horizontally at 2 m s^{-1} near the outlet (fig. 13). The smoke did not flow directly to the outlet. Instead, it moved down the right side of the chamber during the first second and then diffused as it moved upward along the left side. The CFD model prediction was similar to the smoke test (figs. 14a and 14b).

Spray–Fog Grain Surface Deposits

Spray deposits on the grain surface varied with grain height and horizontal proximity to the nozzle (fig. 15). Deposits generally decreased from 0.4 mg cm^{-2} s^{-1} near the

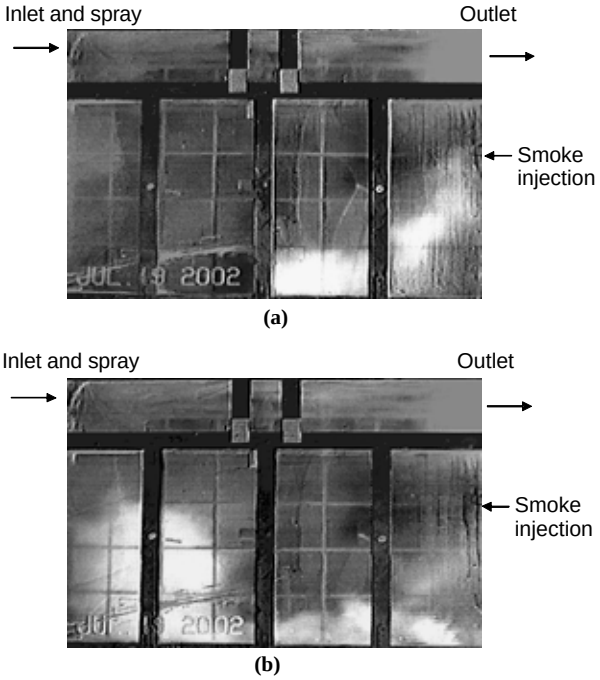

Figure 14. Enhanced video images of the injected smoke cloud and the chamber's recirculating air during spray operation and simplified configuration: (a) after 1 s of smoke injection, and (b) after 2 s of smoke injection.

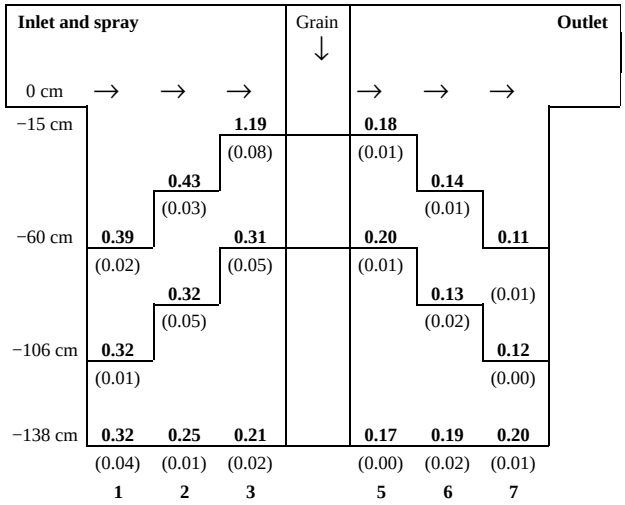

Figure 15. Schematic view of the test chamber and spray deposits.

inner wall to 0.1 mg cm^{-2} s^{-1} near the outlet wall. Higher levels of grain deposits were found nearer to the nozzle. Non−uniformity was more evident as the pile moved closer to and into the spray plume. The heaviest deposit was 1.19 mg cm^{-2} s^{-1} when the peak of the grain moved within the plume of the spray. If all the grain were assumed uniformly coated at a rate of 0.4 mg cm^{-2} s^{-1} (the highest deposit from spray fallout) in this test setup, then approximately 550 g of water would be added to 1500 kg of grain and the grain moisture content would increase by 0.04%. Most stored grain is maintained between 10% to 14% moisture content. A change of moisture by only 0.1% is normally not considered a problem. In addition, after the spray treatment, the grain is further handled and mixed, which helps reduce non−uniformity. The units for deposits on grain were in seconds because the surface of the grain was continually changing with incoming grain. Three levels of grain (−60, −106, and −138 cm) were used for the spray deposit test. The spray deposits are shown at each level and at each sample location (mg cm^{-2} s^{-1}). Standard deviations are in parentheses.

Spray−Fog Sidewall Deposits and Modeling

The test chamber was narrow compared to a full−size grain−receiving hopper. The chamber cross−section was further restricted in the middle by the grain stream. This restriction temporarily increased particle concentrations and impingement on the wall at the middle portion of the chamber. Table 5 gives the experimental fog deposits on the sidewall and above the grain from seven nozzles at 6.9 MPa.

Table 5. CFD−estimated droplets deposited from nozzles (n1, n2, n3) and observed average sidewall deposits from spray.

	CFD Deposit by Nozzle Position[a] (droplets/filter/nozzle)			CFD Relative	Observed Sidewall Deposit (mg cm^{-2} min^{-1})		Observed Relative
Filter	n1	n2	n3	Deposit[b]	Avg,	Std. Dev.	Deposit
m(0)	338	0	0	4.5	11.0	2.8	7.3
m(1)	228	0	0	3.0	5.3	1.2	3.5
m(3)	51	24	0	1.0	1.5	0.3	1.0

[a] Nozzle positions are shown in figures 3 and 6.
[b] Relative deposit was determined by dividing by m(3).

The highest deposits were at the narrowed cross−section, m(0), and decreased with distance from the middle.

CFD−estimated deposits are also listed in table 5. Most of the sidewall deposits came from a single nozzle (n1), which was located closest to the wall. The second and third nozzles from the wall (n2 and n3) had little effect. Like the observed deposits, the particle−tracking model estimated the largest accumulations at the middle of the test chamber, m(0). Observed and predicted relative deposits were 7.3 and 4.5, respectively, for m(0), and 3.5 and 3.0, respectively, for m(1). These differences could be due to the fact that the model used larger sampling surfaces than the experiment and that the spray plume diffused with distance from the nozzle. During the experiment, the 11.4 cm diameter m(0) filter was totally in the spray plume. For the CFD modeling and because of mesh selection, the virtual m(0) sampling surface was larger (30 × 30 cm) than the actual filter and included areas inside and outside the spray plume.

Sidewall spray deposits in the test chamber were larger than expected. However, the grain column was relatively close to the sidewall and caused significant restriction to the airflow. In a full−scale situation, the incoming grain column would have less influence on the sideways movement of the spray fog because the walls would generally be farther away from the incoming grain.

The dust sidewall deposits during spray treatment were higher than for control grain−drop test (table 6). Possibly, the dust and spray droplets had agglomerated and deposited together. In both cases, the grain was delivered at the same rate and duration. During the control case, dust exited the chamber from both the inlet and outlet, with the highest concentration near the exits. During spray operations, the dust deposits (column 4 in table 6) directly correlated with the spray deposits (column 6 in table 5) and were highest in the middle of the chamber. The regression of dust sidewall deposits to spray sidewall deposits correlated with an R^2 greater than 0.95. These deposits were observed above the grain, and any deposits on the walls below the grain were scoured off during grain flow.

Conclusions

The following conclusions were drawn from the study:

- More than 90% of the measured spray−fog droplets ranged from 10 to 40 μm. Droplet velocities were more than 10 m s^{-1} at 7.6 cm and decreased to 4 to 6 m s^{-1} at 30.5 cm from the nozzle.
- Velocity pressures from a single nozzle and 7.6 cm from the orifice were parabolic (with a base diameter of approximately 3 to 4 cm) with maximum pressures over 275 Pa and an average pressure of 200 Pa.
- The CFD model predicted air and grain dust recirculation back toward the entrance in the lower portion of

Table 6. Observed sidewall dust deposits.

	Sidewall Dust Deposit (mg cm^{-2} min^{-1})			
	Control		After Spray Treatment	
Filter	Average	Std. Dev.	Average	Std. Dev.
m(0)	0.2	0.1	1.2	0.2
m(1)	0.3	0.1	0.9	0.1
m(3)	0.4	0.1	0.5	0.2

the test chamber during spray operation and grain receiving. Predicted results qualitatively agreed well with a smoke test showing the movement of smoke and air from the exit toward the entrance.

- Deposits of mist on the grain varied with depth of grain and proximity to the nozzle and generally ranged from 0.1 to 0.4 mg cm^{-2} s^{-1}. The moisture addition to grain from the spray fallout was estimated to be less than 0.04%. Stored grain has normal moisture content around 12%.
- Spray sidewall deposits were 11 mg cm^{-2} min^{-1} at the middle of the test chamber, where the grain column reduced the path, and 1.5 mg cm^{-2} min^{-1} near the outlet. Sidewall dust deposits ranged from 1.2 to 0.5 mg cm^{-2} min^{-1} and correlated to the sidewall spray deposits.

The modeling techniques presented in this study can be extended to optimize the design and operational parameters of airflow and dust control at grain handling facilities or to evaluate and compare existing air collection and dust control methods that have different geometries. In this case, modeling described how to consider airflow and droplet transport from a line of spray nozzles. The models show the change in air circulation and the resulting droplet and particle motion. This airflow helped contain the dust emissions, and grain dust emissions were concentrated near the spray nozzle for maximum spray and dust interaction.

Acknowledgements

This research was supported by the USDA−ARS Grain Marketing and Production Research Center. The mathematical modeling assistance provided by Dr. J. L. Steele and Dr. C. K. Spillman and the technical assistance provided by Dennis Tilley are greatly appreciated.

References

Al−Arifi, A., T. Short, and P. Ling. 2001. Validating the CFD model for air movements and heat transfer in ventilated greenhouses. ASAE Paper No. 014056. St. Joseph, Mich.: ASAE.

Brabec, D. L. 2003. Experimental and numerical modeling of dust control at grain receiving with a high−pressure water−fogging system. PhD diss. Manhattan, Kans.: Kansas State University.

Brabec, D. L., R. G. Maghirang, and M. E. Casada. 2004. Effectiveness of a high−pressure water−fogging system in controlling dust emissions at grain receiving. *Trans. ASAE* 47(2): 505−511.

Brown, R. B., and M. M. Sidahmed. 2001. Simulation of spray dispersal and deposition from a forestry airblast sprayer − Part II: Droplet trajectory model. *Trans ASAE* 44(1): 11−17.

Enarson, D. A., S. Vedal, and M. Chan−Yeung. 1985. Rapid decline in FEV in grain handlers. *American Rev. Respir. Dis.* 132: 814−817.

Federal Register. 1994. Prohibition on adding water to grain. *Federal Register* 59(198).

Fluent. 2002. Computational fluid dynamics software. Lebanon, N.H.: Fluent, Inc.

Hinds, W. C. 1982. *Aerosol Technology: Properties, Behavior, and Measurement of Airborne Particles* . New York, N.Y.: John Wiley and Sons.

Kwok, K. C. 1991. Fundamentals of air−spray painting. PhD diss. Minneapolis, Minn.: University of Minnesota.

Office of Technology Assessment. 1995. Technology and policy for suppressing grain dust explosions in storage facilities. OTA−BP−ENV−177. Washington, D.C.: U.S. Congress, Office of Technology Assessment.

Reid, R. G. 1987. The effects of the use of oil on wheat milling. AOM Technical Bulletin 1987: 4981−4985. Leawood, Kans.: Association of Operative Millers.

Schoeff, R. W. 2002. Agricultural dust explosions in 2001. January newsletter. Manhattan, Kansas: Kansas State University, Department of Grain Science.

Spraying Systems. 2000. Technical bulletin: Drop−size measurement. Wheaton, Ill.: Spraying Systems Co.

Sun, H., R. R. Stowell, H. M. Kenner, and F. C. Michel. 2002. Two−dimensional computational fluid dynamics (CFD) modeling of air velocity and ammonia distribution in a high−rise hog building. *Trans ASAE* 45(5): 1559−1568.

Tsay, J., H. E. Ozkan, R. D. Brazee, and R. D. Fox. 2002. CFD simulation of moving spray shields. *Trans ASAE* 45(1): 21−26.